Sensory convergence in the world's largest cavefish diversification: patterns of neuromast evolution, distribution and associated behaviour in *Sinocyclocheilus*

Bing Chen[1], Tingru Mao[1], Yewei Liu[1], Wenzhang Dai[1], Xianglin Li[1], Amrapali P. Rajput[1], Jian Yang[2], Joshua B. Gross[3], Madhava Meegaskumbura[1*]

[1] Guangxi Key Laboratory for Forest Ecology and Conservation, College of Forestry, Guangxi University, Nanning, Guangxi, China

[2] Key Laboratory of Environment Change and Resource Use, Beibu Gulf, Nanning Normal University, Nanning, Guangxi, China

[3] Department of Biological Sciences, University of Cincinnati, Cincinnati, OH 45221, U.S.A.

Corresponding author *E–mail* : madhava_m@mac.com

Abstract

The genus *Sinocyclocheilus* represents the largest freshwater cavefish genus in the world. This emerging model system is endemic to the southern Chinese karstic landscape, and demonstrates multiple adaptations for caves (troglomorphism), with eye-degeneration being the most pronounced. The less-apparent lateral line system, which is often expanded in cave-dwellers, has been studied in other cavefish systems, but never in the context of this diversification. Here we investigated the distribution and evolution of cephalic neuromasts in 26 *Sinocyclocheilus* species. We used live-staining and behavioural assays, and interpreted results in a phylogenetic context. We show that asymmetry in neuromast features and the rate of evolution is greater in cave-adapted species. Ancestral state reconstructions show that most *Sinocyclocheilus* are right-biased with some scatter, and show convergence of neuromast phenotypes. There is substantial variation in cephalic neuromast distribution patterns between and (to a lesser extent) within species. Behavioural assays show blind species have a distinctive wall-following behaviour. We explain these patterns in the context of the deep evolutionary history associated with this karstic region, other organismal traits, and habitat occupation of these remarkable diversifications of fishes. Interestingly, some of these neuromast patterns and behaviour show convergence with other phylogenetically distant cavefish systems.

Key words: Asymmetry, convergence, ancestral state reconstructions, wall-following behaviour, live staining, troglomorphisim

Background

Cave-dwelling (hypogean) fish provide a valuable system to study evolutionary novelty [1-4], owing to the extreme conditions associated with these habitats, such as limited food and perpetual darkness. Strong selective pressures arising from this extreme environment are associated with a suite of regressive morphological changes, such as loss of eyes and pigment [5, 6]. However, numerous constructive features also evolve in cave-dwellers. Among the most notable are expansions of the mechanosensory lateral line system [7]. Here, we examine the evolution of the lateral line system in the species-rich genus *Sinocyclocheilus*, an emerging model system and the largest diversification of freshwater cavefish in the world [8, 9].

Neuromast organs are composed of hair cells with cilia embedded in a gelatinous cupula, surrounded by a complex set of support cells [10, 11]. There are two general neuromast types: canal neuromasts (CN), which are larger, and embedded in a bony canal, and superficial neuromasts (SN), which project directly from the skin epithelium [12-14]. In the Mexican tetra (*Astyanax*), cave morphs harbor variation in the number and size of both types of neuromasts in the lateral line, including several-fold more SNs compared to surface fish. Moreover, *Astyanax* cave morphs have a highly asymmetric distribution of neuromasts across the left/right axis compared to surface-dwelling morphs [15]. At present, it is unclear the relevance of this asymmetry, however, some studies suggest it facilitates lateral swimming preference, rheotaxis (orientation towards flow), foraging, shoaling, predator avoidance, and mate-finding [7, 16-20].

Sinocyclocheilus are distributed across a vast 62,000 km^2 karstic area in Yunnan

and Guizhou Provinces and Guangxi Zhuang Autonomous Region [21, 22]. Based on their habitat preference, these fish can be divided into three principal groups: troglobitic (cave-restricted); troglophilic (cave-associated); and surface-dwelling [9]. However, one study characterized neuromast size differences between two *Sinocyclocheilus* species [20]. *Sinocyclocheilus* species span the macroevolutionary transition from surface to cave-restricted species and thus offer an exceptional opportunity to examine the evolution of traits associated with this transition.

Here we examined numerical variation, lateral distribution and behavioural differences associated with neuromasts in *Sinocyclocheilus*. Neuromasts may provide functional compensation for eye loss, therefore we hypothesized that more severe eye/vision loss may be associated with compensatory expansions of the lateral line neuromasts. Specifically, troglomorphy was predicted to be associated with more, and larger, neuromasts. Additionally, we anticipated a higher prevalence of distributional asymmetry of neuromasts in troglomorphic species compared to surface species, owing to relaxation of symmetry.

We found that neuromast distributions were asymmetric among all groups, however the degree of asymmetry was most apparent for Regress-Eyed (troglomorphic; collectively both Blind and Micro-Eyed) species. Additionally, in phylogenetic contexts the pace of neuromast evolution is faster among species with smaller eyes, compared to normal eyed species. Taken together, this work provides the first diversification-wide description of lateral line evolution, and clarifies the shared evolutionary pressure on constructive trait evolution among distantly-related species that colonize caves.

2. Methods

Sinocyclocheilus adult fishes used in this study were examined using live, biosafe staining techniques and behavioural assays. The project was approved by Guangxi Autonomous Region Government and Guangxi University Ethical Clearance Committee (# GXU-2021-125).

(a) Fish maintenance in captivity

Adult fish used in this study were collected from the field from 2017-2020 across Yunnan and Guizhou Provinces and Guangxi Zhuang Autonomous Region of China (figure 1, see geographic coordinates in electronic supplementary material: table S1, figure S5). All fish were maintained in a centralized fish aquarium system, and maintained at (pH: 7.0 - 8.0, temperature 19°C ± 1°C, dissolved oxygen 8.5mg/L). Specimens larger than 5 cm were maintained in large glass aquaria (90 × 50 × 50 cm, 150 × 80 × 80 cm), with individual mechanical and bio-filters. For this study, 76 individuals from 26 *Sinocyclocheilus* species were used (table 1). *Carassius auratus* (n = 3) and *Cyprinus carpio* (n = 3), two species from a closely related clade to *Sinocyclocheilus* for comparison.

104

105

106 **Table 1.** Summary of 26 *Sinocyclocheilus* species used in the current analysis grouped

107 according to eyes morphology and habitat.

	Troglobitic (TB)	**Troglophilic (TP)**	**Surface (S)**
Blind (B)	*S. furcodorsalis* *S. tianlinensis* *S. tianeensis* *S. xunlensis*		
Micro-eyed (ME)	*S. mashanensis* *S. altishoulderus* *S. microphthalmus* *S. bicornutus* *S. rhinocerous* *S. cyphotergous*	*S. multipunctatus*	
Normal-eyed (NE)	*S. guilinensis* *S. huanjiangensis* *S. macrophthalmus* *S. guanyangensis* *S. brevis* *S. lingyunensis* *S. zhenfengensis* *S. jii* *S. yishanensis*	*S. longibarbatus*	*S. angustiporus* *S. oxycephalus* *S. malacopterus* *S. purpureus* *S. maitianheensis*

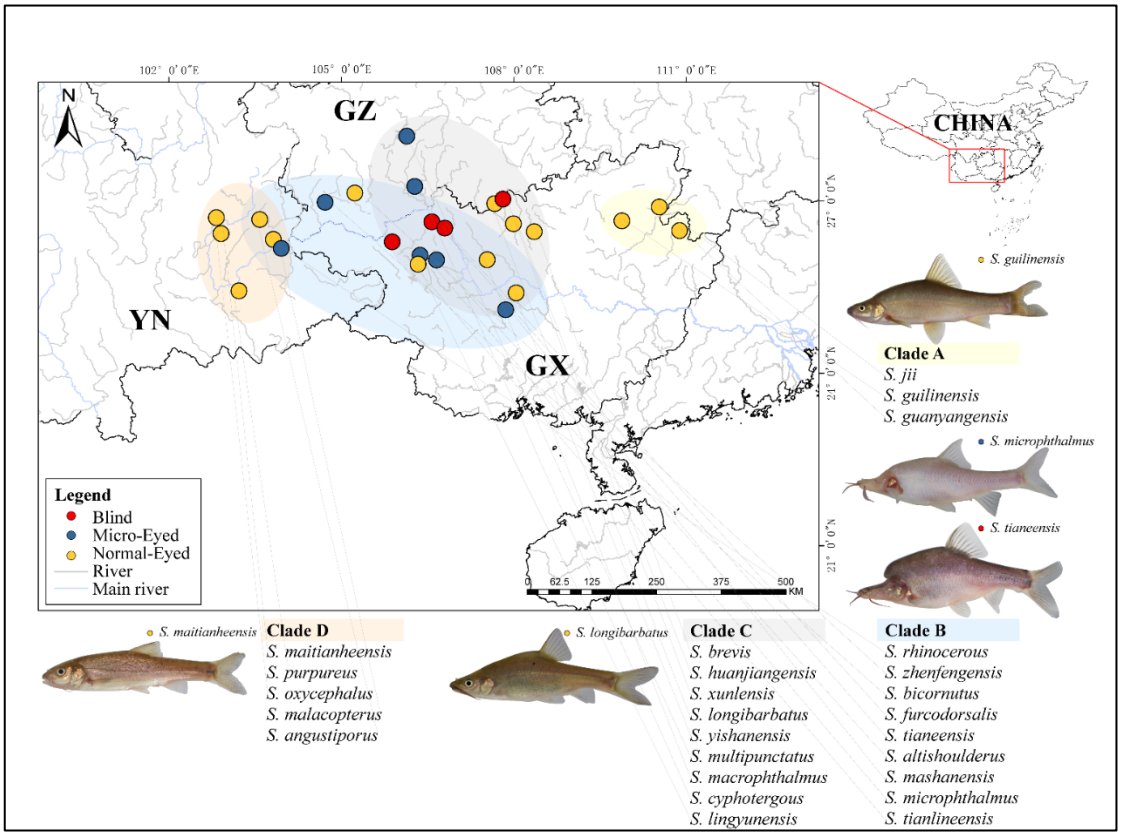

Figure 1. Map showing the distribution of sampling sites of the 26 species of *Sinocyclocheilus* (n = 76) used in this study. These fishes are mainly distributed across South China's Karstic habitats on three provinces: Guangxi Autonomous region (GX), Guizhou (GZ) and Yunnan (YN). The four main clades (A – D, represented by a color code), the species used from each clade, and a representative photo of species from these clades are shown. Early emerging Clade A is mainly distributed in the eastern range of the diversification and Clade D to the hills to the West; Clade B and C contain the most troglomorhpic species and are distributed mainly across GX and GZ. The eye-condition (Blind, Micro-eyed and Normal-eyed) are depicted using a color code.

(b) Vital staining of neuromasts

To visualize bones and neuromasts, live fish were immersed in 1mg/L Calcein-AM

(C0875-5G; Sigma-Aldrich) and 20μg/ml DASPEI (D0815; Sigma-Aldrich) [15, 23, 24]. Fish were anesthetized using MS222 (E808894-5g; Macklin) 0.01-0.02g/L for 3-6 min followed by brief immersion in ice water for ~20s, depending on size and age (e.g., smaller specimens were exposed to ice water for shorter periods). All individuals were continuously monitored to ensure the health and safety of experimental individuals.

(c) Digital Analysis of Neuromast Position and between Distances

This study focused on the cephalic region anterior to the opercular and interopercular bones, near the arc on the lateral aspect [20, 22]. Images were collected using a Leica M165FC fluorescent stereomicroscope outfitted with Leica Application Imaging software (LAS X v3.4.2.18368). The dorsal, left and right aspects of each individual were imaged under identical conditions. High-definition "montage" image were consolidated following automated alignment and 'flattening' of 30 images collected in the z-plane (× 9/ 13/ 16 magnification) using LASX or Helicon Focus (Pro v7.6.1), to perform the two-dimensional shape images. The use of montage imaging minimized potentially confounding variables arising from the z-plane for each specimen.

The outline of fish and neuromast positions were obtained using the "Pencil" and "Point" tool in GIMP (v2.10.24). Neuromast numbers were quantified using an automated method in ImageJ (v1.8.0), following the method of Gross et al. (2016) [15]. For ambiguous images, we performed direct, manual counting (figure 3*a*). We calculated the size (2-D area) of individual neuromasts, lens, and eye orbit diameter by determining their size in pixels using the "measure" function in ImageJ and converting to mm^2. We also used a vernier caliper to measure standard length (SL). To determine

the density of neuromast within particular unit areas, we used "Delaunay Voronoi" triangulation in ImageJ to define a proxy for the mean distance between neuromasts [25-27] (figure 3*a*).

(d) Quantifying symmetry

To examine positional symmetry of neuromasts across the left-right axis, we manually superimposed the fluorescent images of neuromasts (figure 3*b*). We used excitation filters for three colors (Blue 470/40 nm, Texas Red 560/40 nm and Green 546/10 nm). In GIMP, we then reflected the left images to align with the right images, creating a single image. We measured the scoring of neuromasts in the reverse sequence (right-side first) relative to the initial scoring of neuromasts (left-side first) to avoid bias in our calculations [28].

The "colocalization" [29, 30], and "JACop" [31, 32] plugins in FIJI were used to calculate an asymmetry coefficient [15, 33, 34]. We performed a Pearson's correlation to compare the intensity distribution between channels [35]. Next, we calculated an Overlap Coefficient (OC), to identify positional overlap of signals from the left and right sides [36]. This enabled us to quantify the extent to which positions of neuromasts on the left and right sides of the cranium were symmetric (figure 3*a*).

We divided 26 species into Regressed-Eyed groups (containing Blind: n = 12 and Micro-Eyed: n = 21) and Normal-Eyed groups (n = 45), following the categorization and phylogeny of Mao et al. (2021). Importantly, a few *Sinocyclocheilus* species do not have uniform eye sizes [22]. For instance, *S. guanyangensis* have highly variable eye sizes, so for this study we selected individuals with the most common Normal-Eyed

165 morphology. All parametric neuromast measures were subjected to one-way ANOVA
166 with a post-hoc Tukey test analysis. Non-parametric distributions were subjected to
167 Wilcoxon Signed Rank Test (2-tailed, Holm correction) or a Kruskal-Wallis test with a
168 post-hoc analysis Dunnett test (2-tailed, Bonferroni correction). Statistical significance
169 was set at $p < 0.05$. We used the packages "wmc" and "FSA" in R (v3.6.3). Principal
170 Component Analysis (PCA) was used to evaluate the following variables: number, area,
171 asymmetry coefficients and mean distance. To analyse the relationships between
172 Regressed-Eyed and Normal-Eyed groups, we performed Spearman's rank correlation
173 coefficients using SL, eye traits, area, number, mean distance and OC of neuromasts
174 patterns.

175 **(e) Phylogenetic inference**

176 To study the patterns of neuromast evolution in *Sinocyclocheilus,* we inferred a
177 phylogenetic tree for the 26 species, using two available gene fragments from Genbank
178 (NADH-ubiquinone oxidoreductase chain 4 - ND4 and cytochrome b gene – Cyt b),
179 together with an outgroup species (*Cyprinus carpio*) (table S1). We used two different
180 methods for phylogenetic inference [37] – Bayesian and Maximum Likelihood for tree
181 construction (alignment, model selection and phylogenetic inference method details are
182 available in the electronic supplementary material, Supplementary Methods).

183 **(f) Evolution rate analysis**

184 To test the allometric evolution rate between neuromasts in different morphs [9],
185 we analysed neuromast numbers, left/right-side numbers, mean distance coefficient,
186 area and density (i.e. the proportion of number and area anterior to the gill). We used

100 potential trait histories from stochastic character mapping, and fit two alternative models (single or multiple rate model, calculated by AIC) of evolution for each studied trait. In the case of small samples, we assumed the AIC and AICc to assess, and then weighted from Bayesian analyses on the trees using the brownie.lite function. We used the package "rgl", "ape" and "phytools" in R to calculate the model-averaged estimates [38].

(g) Patterns of neuromasts evolution using ancestral state reconstructions

To understand the broad patterns of neuromast evolution in *Sinocyclocheilus*, we classified 26 species into the following three morphological groups: (1) Left-right axis asymmetry: according to different degree of overlapping coefficient, divided as Absolute-asymmetry (OC < 0.1) and Slight-asymmetry (OC ≥ 0.1) based on Gross et al. (2016) [15]. (2) Left/right-bias handedness: we used the normalized SN number by signed (directional) asymmetry rate: $\mathrm{SAR} = \frac{R-L}{R+L} \times 100\%$ following Planidin et al. (2021) [39], which suggests the presence of two morphological categories: Right-biased (SAR > 0, neuromasts on right-side mainly) and Left-biased (SAR < 0, figure S1). (3) Distance expansion: depending on the results of neuromasts mean distance coefficient, we divided species into Scattered (DEL > 0.2) and Serried (DEL ≤ 0.2), following Gross et al. (2016) [15] (table S1).

To understand the evolution of neuromast patterns, we performed ancestral state reconstructions using these three morphological categories. One hundred stochastic reconstructions were simulated through the stochastic mapping approach that was conducted using function "make.simmap" (model = "ER") in the R packages "ape",

209 "phytools" and "viridisLite".

210 **(h) Cave-dwelling behaviour associated with neuromast variation**

211 To understand how neuromast patterns may facilitate certain behaviour, we carried out
212 a series of behavioural assays. All assays were performed using the following 14 species
213 (n = 3 individuals for each): Blind - *S. furcodorsalis, S. tianlinensis, S. tianeensis*;
214 Micro-Eyed - *S. mashanensis, S. microphthalmus, S. bicornutus, S. multipunctatus*;
215 Normal-Eyed - *S. guilinensis, S. longibarbatus, S. macrophthalmus, S. oxycephalus, S.*
216 *zhenfengensis, S. purpureus, S. maitianheensis*. Each experimental fish was
217 acclimatized for 30 min in a rectangle assay arena (45 × 28 × 28 cm) in system water.
218 An infrared camera (Cannon XF400/405) was used to capture video under infrared light
219 in a quiet, dimly lit room (frame rate: 4Mbps (VBR, YCC 4:2:0, 25p, 1280 × 720).

220 Wall-following behaviour has been observed in *A. mexicanus* cavefishes; therefore,
221 we examined a range of wall-following within the arena. This included fish swimming
222 a minimum distance of its SL along the wall, or a distance of ≤ 0.5 SLs away from the
223 wall (figure 5*a-b*) [40, 41]. We recorded normal tracking without stimulation for 10-
224 min to determine if wall-following behaviour was present using EthoVision XT (v15.0 ,
225 Noldus) alongside direct visual monitoring. (2) We next used an aeration pump (45~50
226 Hz vibration) for 5-min to record the approaching of a novel object in modified
227 vibration attraction behaviour test [42-44]. We selected the area centered on the
228 stimulation model based on tank shape (10 × 16 cm). We monitored the frequency of
229 time spent in the stimulation range from left/right-side. Data analysis were performed
230 in R's basic functions as mentioned.

Results and Discussion

Neuromast distribution is asymmetric in all cave fish studied to date [15, 45-48]. Accordingly, we found the two outgroup species of Cyprinidae showed several neuromasts on observation region, which did not show a comparable pattern of neuromast asymmetry as was observed in *Sinocyclocheilus*. Fish living in perpetual darkness frequently lose vision while enhancing non-visual sensation, such as the lateral line [42, 49, 50]. Here, for the first time, we show that *Sinocyclocheilus* similarly conform to this pattern (figure 2). Additionally, widespread neuromast distributional asymmetry in *Sinocyclocheilus* is convergent with other distantly related cavefish species inhabiting similar cave microenvironments. Interestingly, our results showed that this asymmetric neuromast pattern is variable across the 26 *Sinocyclocheilus* species tested, with most species demonstrating a right-sided bias (figure 4). Evidence for neuromast asymmetry patterns in other lineages comes from two lineages from Central and North America: *Astyanax mexicanus,* with a left-side bias and the *Gasterosteus aculeatus* (stickleback fish), with a right-side bias [39, 51]. These convergent results reveal variation in "sidedness" across taxa, despite convergence in the asymmetry of neuromasts traits.

(a) Patterns of neuromast symmetry and asymmetry

The neuromasts distribution pattern showed asymmetry across the left-right axis, with variation both within and across species (figure 2*a*, table S2). Interestingly, mean overlap coefficients indicated that all species showed a degree of neuromast asymmetry.

253 Normal-Eyed species showed the least asymmetry, while Blind species showed the
254 highest and Micro-eyed species had intermediate values (mean ± s.d.: Normal-Eyed =
255 0.098 ± 0.05; Blind = 0.091 ± 0.031; Micro-eyed = 0.096 ± 0.027; $H_2 = 0.64$, $p > 0.05$).
256 This finding is consistent with prior work suggesting that asymmetry may facilitate
257 navigation in darkness [52, 53], foraging [54] and the ability to maximize sensory
258 information using fewer receptors [39, 51]. In comparing asymmetry measures across
259 clades, Clade D (all Normal-Eyed, surface-dwelling species, showed the least
260 asymmetry (mean ± s.d. = 0.119 ± 0.058), while Clade C (mean ± s.d. = 0.079 ± 0.031)
261 showed the highest asymmetry; with Clade A and B demonstrating intermediate values
262 (Clade A – 0.086 ± 0.029 and Clade B – 0.104 ± 0.038).
263

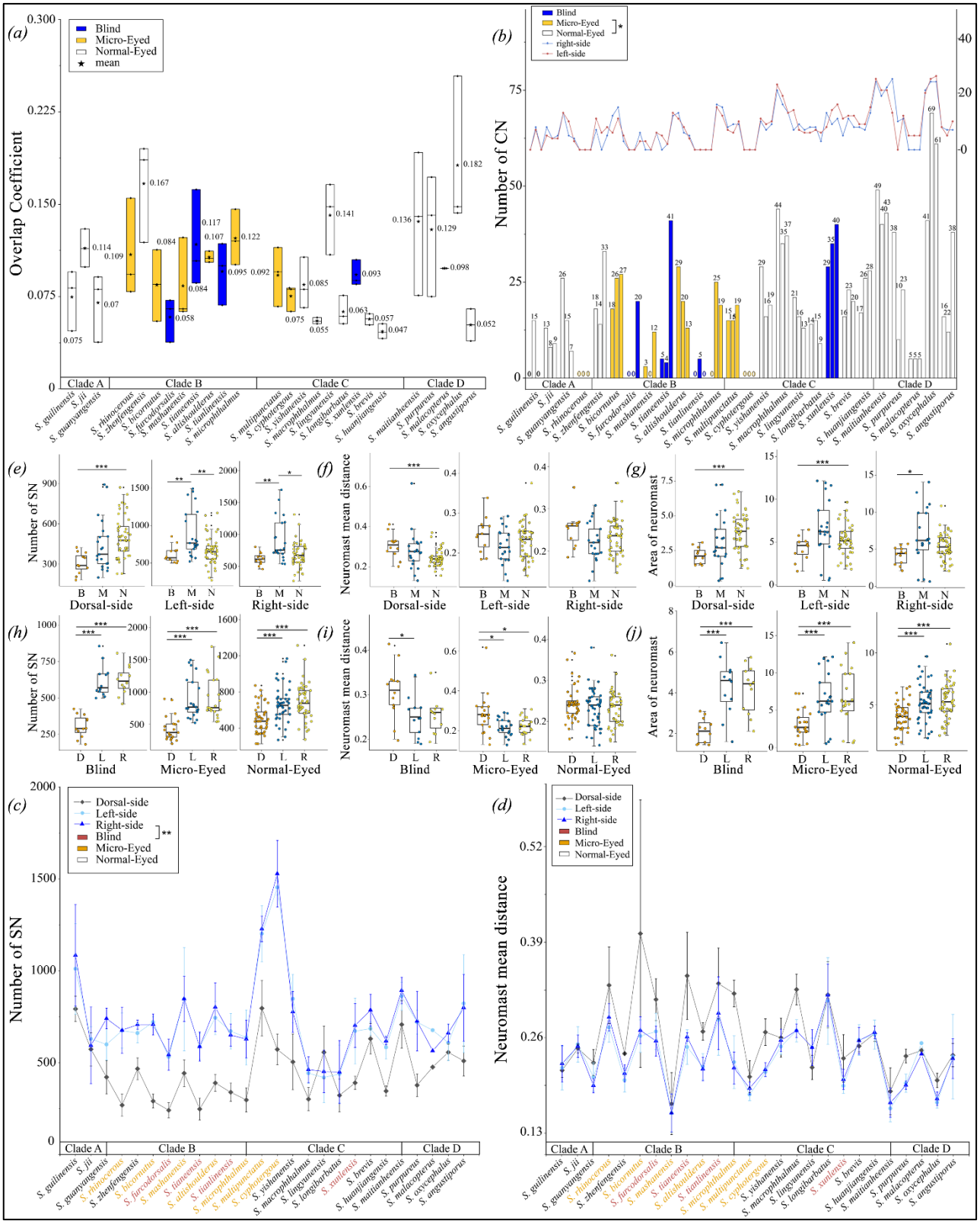

Figure 2. Comparison of neuromast-related measurements for 26 species of *Sinocyclocheilus* (n = 76).

(a) The average scores of Overlapping Coefficient (OC) measured as the pattern of

neuromasts on left/right-side of the fish. The standard of asymmetry results is defined as: asymmetry (OC < 0.1), symmetry (OC ≥ 0.1). Clade A-D represent the clade level relationships of these 26 species in the phylogenetic tree. All statistical results are available in table S1, S2.

(b) The bars represent the individual's canal neuromasts (CN) total counts and the lines represent the left and right sides of cephalic CN in different species. The CN of Micro-Eyed species was significantly less than Normal-Eyed species ($H = -2.64$, $p = 0.025$).

(c) The mean number of superficial neuromasts (SN) on the cephalic area (dorsal, left and right sides) in different *Sinocyclocheilus* species.

(d) The mean surface area covered by SN on the dorsal/left/right-side of different *Sinocyclocheilus* species. The surface species covered by the dorsal SN are less than that of the surface are covered by the right and left sides of fish.

(e-g). The comparisons about: (e) the number of SN; (f) neuromasts mean distance coefficient; (g) area of SN on Dorsal/Left/Right-side on cephalic area. Group divided by the Blind (B in orange), Micro-Eyed (M in blue) and Normal-Eyed (N in yellow). The Wilcoxon signed rank (2-tailed, Holm correction) test suggested that the surface covered by dorsal neuromasts are significantly less than that covered by the right and left sides. *: $P < 0.05$, **: $P < 0.01$, and ***: $P < 0.001$. All statistical results are available in table S2, S5.

(h-j). The comparisons of the non-parametric statistical tests performed for (h), the mean number of SN; (i) neuromasts mean distance coefficient; (j) mean area of SN on the cephalic area of the Blind, Micro-Eyed and Normal-Eyed morphs. The comparisons

were sub-divided into dorsal-side (D in orange), left-side (L in blue) and right-side (R in yellow) for visualization purposes.

(b) Patterns of neuromast distribution

Generally, we found more SNs on the right compared to the left-side, however we observed substantial variation between and across species. In the dorsal aspect, Blind fish have the fewest, Normal-Eyed fish have the most, and the Micro-Eyed group was intermediate (figure 2*e*). Unexpectedly, there were significantly fewer SNs in Blind species (mean ± s.d.: Blind = 1543 ± 248; Micro-Eyed = 2252 ± 802; Normal-Eyed = 1859 ± 504; $H_2 = 10$, $p = 0.0065$, table S5). In terms of lateral distribution, Blind and Normal eyed fish had higher numbers on the right-side, while Micro-Eyed species had more neuromasts on the left-side (median: left = 767, right = 758; $W = 227$, $p = 0.890$; figure 2*h*; table S5).

We found that dorsal neuromast numbers are significantly lower than the lateral sides. An interesting exception was *S. lingyunensis* (N-TB, Clade C), dorsally distributed neuromasts outnumbered laterally-situated neuromasts (mean dorsal = 557, left = 419, right = 453; figure 2*c*, table S5). In the dorsal aspect, Normal-Eyed species had the most neuromasts, while the Blind group had the fewest. One potential explanation for this difference could be that obligate subterranean fishes experience relaxed selective pressure (e.g. aerial predation from birds) [21, 55], but perhaps dorsal neuromasts are necessary for navigation within caves [56].

With respect to neuromast expansion (scatter), we found that the most scattered

SNs are dorsal, especially in Blind species (mean ± s.d.: Blind = 0.31 ± 0.06; Micro-Eyed = 0.28 ± 0.10; Normal-Eyed = 0.24 ± 0.04; H_2 = 12, p = 0.002; figure 2*f*, table S5). Additionally, neuromasts tend to be more scattered on right- compared to the left-side across all three groups (median right/left Blind = 0.26, 0.25; Micro-Eyed = 0.22, 0.21; Normal-Eyed = 0.24, 0.23; figure 2*d*). Interestingly, the Blind cavefish group demonstrated the most scatter, while the Micro-Eyed group had the least scatter (figure 2*i*, table S5). The Mexican cavefish (*Astyanax mexicanus*) demonstrates more scatter in the surface forms compared to *Sinocyclocheilus* [15, 57], however this is likely due to the fact that *Astyanax* Blind forms have more neuromasts, and hence less scatter.

In the comparison of surface area covered by neuromasts, we found a significantly lower surface area populated by neuromast on the cephalic region dorsally, with the Blind group having the smallest area (mean ± s.d. Blind = 2.14 ± 0.59; Micro-Eyed = 3.13 ± 1.94; Normal-Eyed = 3.88 ± 1.33; H_2 = 15.9, p = 0.0003; figure 2*j*). When comparing lateral sides, we found the total distributional area of neuromasts to be highly comparable within groups (median right/left-side Blind = 4.44, 4.6; Micro-Eyed = 6.19, 6.21; Normal-Eyed = 5.31, 5.14; table S5). Normal-Eyed species have the largest area of neuromast distribution, Micro-Eyed fish have an intermediate area, and the Blind group had the smallest area covered by (mean ± s.d. = 10.56 ± 2.95; Micro-Eyed = 16.44 ± 8.80; Normal-Eyed = 14.49 ± 4.59; F = 3.83, p=0.026; figure 2*g*). Although it has been shown that the neuromast complexity of the Blind species is greater than Normal-Eyed species [20], this however, has not been established at a diversification-wide scale.

Blind *Sinocyclocheilus* have fewer CNs compared to Normal-Eyed *Sinocyclocheilus* (median Blind = 5, Micro-Eyed = 13; Normal-Eyed = 17; table S5), reflecting the same pattern as SNs. For *Astyanax*, surface fish are invariant in terms of numbers, but cavefish are highly variable. Surprisingly, two species, *S. rhinocerous* and *S. cyphotergou* appeared to possess no CNs (both M-TB, figure 2*b*), suggesting the canal lateral line system may have regressed in this species. Interestingly, a similar phenomenon has been observed in Amblyopsid cavefish (Teleostei: Percopsiformes) [47] and in Threespine Sticklebacks (*Gasterosteus aculeatus*) [58].

In sum, neuromasts are generally reduced in number and area in Blind species, but not in distribution (expansion). Somewhat surprisingly, Micro-Eyed species had the most neuromasts, greater area, and least dense distribution of neuromasts. We propose that Blind species may have optimized adaptation to the subterranean biome by using fewer, but more complex, neuromasts. Blind *S. tianlinensis*, for instance, have SNs with greater diameters and more hair cells compared to Normal-eyed *S. macrophthalmus* [20].

(c) Correlations between asymmetry and eye condition

We performed a Spearman Rank's correlation of the highly loading variables for the Regressed-Eyed and Normal-Eyed. In the Regressed-Eyed group, eye measures demonstrated a significantly positive correlation with neuromasts number ($\rho = 0.7$, $p < 0.001$) and area ($\rho = 0.7$, $p < 0.001$) , but a slightly negative correlation with mean distance between neuromasts ($\rho = -0.3$, $p < 0.05$). In the Normal-Eyed group, eye measures had a significantly positive correlation with neuromasts area ($\rho = 0.4$, $p <$

0.005) and mean distance (ρ= 0.4, p < 0.05) , but significantly negative correlation with the results of asymmetry (ρ= -0.4, p < 0.001; figure 3*d,e*, table S4). Overall, the Regressed-Eyed group is more asymmetric compared to Normal-Eyed group.

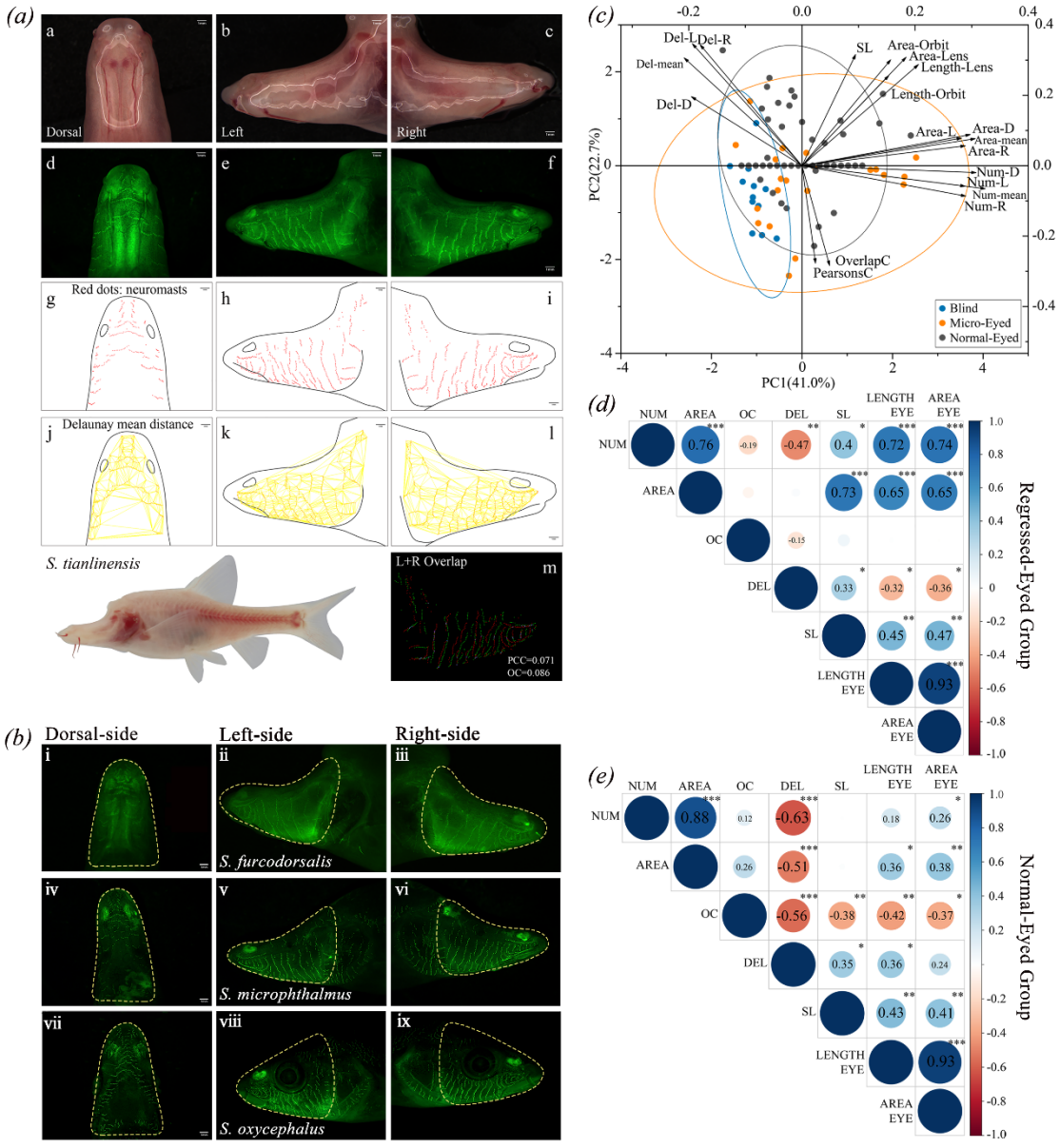

Figure 3. Summary of fluorescent staining results for different cavefish morphs.

(a) the fluorescent staining results of *S. tianlinensis* (Blind species-Troglobitic, B-TB). (table 1 & table S1).

(a-c) photos taken under normal lights. (d-f) dorsal, left and right sides of the

364 neuromasts under fluorescent light. (small green dots are SN, bigger green dots are CN).
365 (g-i) The diagrammatic representations of the dorsal, right and left side neuromasts.
366 SNs denoted by red dots and the area outlined in black represent cephalic region and
367 the olfactory area. (j-l) The neuromasts mean distance measures as the "Delaunay Mean
368 Distance" are indicated by yellow lines. (m) The asymmetry values calculated by
369 overlap coefficient. Red and green dots represent the left and right sides of the fish.
370 Note that the scale of the images is the same at the length of 1.0 mm.
371 (b) The results of the fluorescent staining of three cavefishes, (i-iii) *S. furcodorsalis,*
372 (iv-vi) *S. microphthalmus* and (vii-ix) *S. oxycephalus,* used as representatives of each
373 eye-related morphs. These three species are classified as (B-TB), Absolute-
374 asymmetry/Scattered/Left-bias; (M-TB), Slight-asymmetry/ Scattered/Right-bias and
375 (N-S), Slight-asymmetry/Serried/Right-bias respectively. Scales of the images are the
376 same at the length of 1.0 mm.
377 (c) Principal Component Analysis (PCA) bi-plot for the distribution traits of neuromasts
378 in *Sinocyclocheilus*.
379 The dorsal/left/right-side and mean counts number (Num-D, Num-L, Num-R, NUM);
380 dorsal/left/right-side and mean distance coefficient (Del-D, Del-L, Del-R, DEL);
381 asymmetry coefficients of neuromasts (PearsonsC, OverlapC); eyes traits (area of
382 lens/orbit (Area-Lens, Area-Orbit) and length of lens/orbit (Length-Lens, Length-
383 Orbit)) with standard length [5] were included as variables in the PCA. All results are
384 available in Supplemental table S2, S3.
385 (d) The Correlations between SN number (NUM), area (AREA), mean distances

386 coefficient (DEL) and asymmetry coefficient (OC) of neuromasts; standard length [5]
387 and the length of lens (LENGTHEYE) and area of lens (AREAEYE). The scores
388 indicate the results of the spearman's rank correlation coefficient |ρ|; < 0.3 = no
389 correlation, 0.3-0.8 = low correlation, > 0.8 = high correlation. Positive correlations (ρ >
390 0) and negative correlations (ρ ≤ 0) are shown in blue and red colors respectively. *: P
391 < 0.05, **: P < 0.01, and ***: P < 0.001 indicate the level of statistical significance. All
392 results are available in table S4.
393
394 **(d) Dimensionality of the neuromast variables**
395 We performed a principal component analysis (PCA) based on 26 species of
396 *Sinocyclocheilus* and their neuromast-related variables, to identify key features
397 underlying neuromast variation. Variation on PC1 was explained mostly by the number
398 of neuromasts (mean number: NUM, counts on dorsal side: Num-D) and the total
399 neuromast distributional area (AREA). PC2 was explained mostly by the distances
400 between neuromasts (mean distance coefficient on left side: Del-L, on right side: Del-
401 R; table S3). The 95% confidence intervals for each group shows that intraspecific
402 variation in the Blind group was the narrowest, while the Micro-Eyed group showed
403 the highest variation (figure 3*c*). This may be explained by the fact that Micro-Eyed
404 forms are subjected to selective pressures of both surface habitats, subterranean habitats
405 and the transitional habitats between these [22, 59, 60]; i.e. habitat heterogeneity.
406
407 **(e) Patterns of neuromasts evolution**

We next performed an ancestral reconstruction for three character states: asymmetry, handedness and neuromasts expansion. We found the deeper nodes in the phylogeny showed ambiguity for asymmetry and handedness (see maximum credibility tree; figure 4). However, the deeper nodes for neuromast distribution suggested a scattered distribution of neuromasts is the ancestral condition. In *Sinocyclocheilus,* ~ 70% of the species examined demonstrate right-handedness. Our ancestral state reconstruction shows an entire clade of 7 species is right-handed. However, both left- and right-handed mixed clades and sister taxa are present within the diversification, suggesting this is a variable trait. In contrast, ancestral state reconstructions show nearly 80% of the *Sinocyclocheilus* have scattered neuromast distributions. Additionally, all Blind species showed a scattered neuromast pattern of distribution. (figure 4*c*; black arrow).

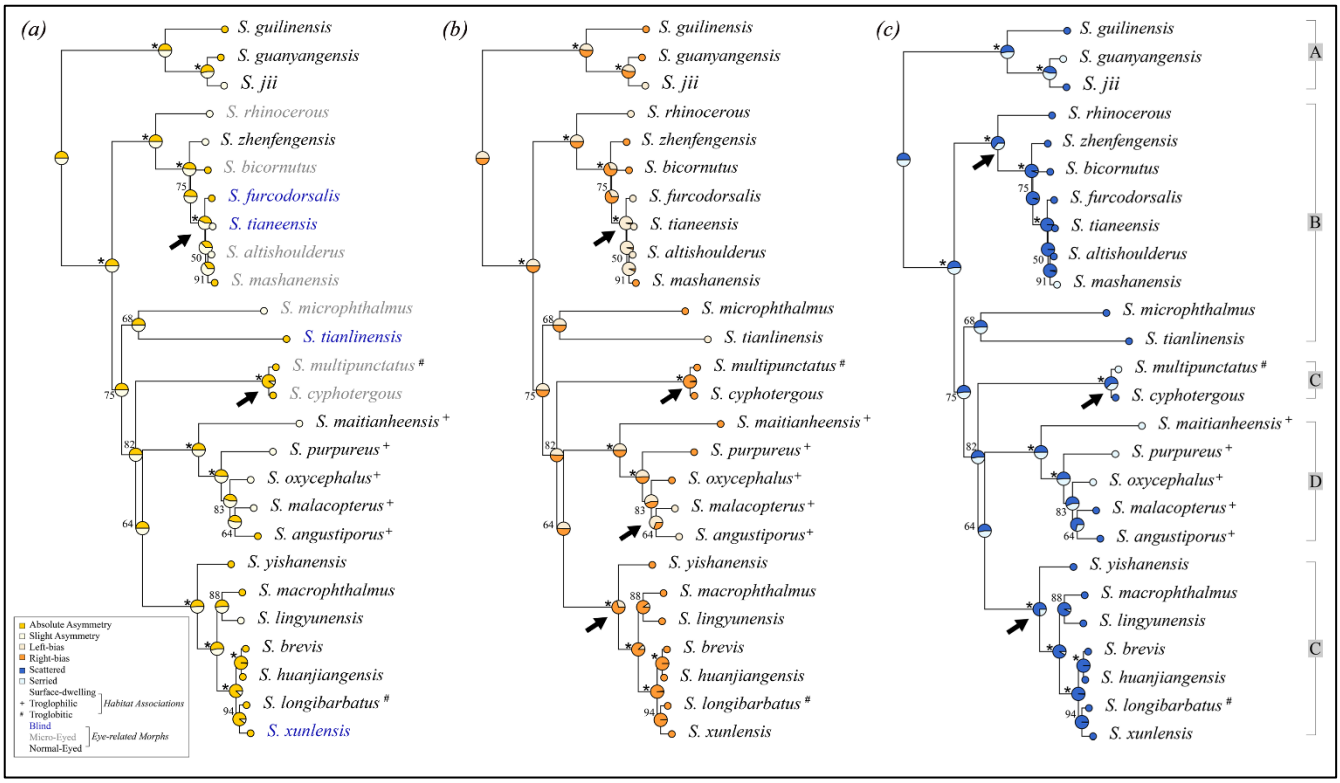

Figure 4. Patterns of cephalic neuromast trait evolution of *Sinocyclocheilus* based

on ancestral state reconstruction on the maximum-likelihood tree. Ancestral state reconstructions based on the Bayesian inference method is shown in figure S2-S4.

(a) Ancestral state reconstruction using stochastic character mapping for symmetry in neuromasts pattern (Absolute/Slight-asymmetry). The tip colors represent state of the extant species and each node indicates the ancestral state as a proportion of the tip state. A, B, C and D showed on the extreme right of the figure indicate four major clades. The bootstrap values > 95% are indicated as * on nodes.

(b) Ancestral state reconstruction using stochastic character mapping for handedness bias (Left/Right-bias) on the phylogeny.

(c) Ancestral state reconstruction using stochastic character mapping for neuromast expansion (Scattered/Serried) on the phylogeny.

(f) Evolution rates analysis

Among cavefish, the rate of neuromast evolution has only been determined for *Sinocyclocheilus.* The rate of scatter for Blind species is higher compared to others (mean distance and density - 3.5 and 6.8 times increased than Normal-Eyed species), and the rate of numerical expansion of neuromasts is 1.2 times greater in Micro-Eyed species (table 3). Normal-Eyed *Sinocyclocheilus* species demonstrated lower evolutionary rates for every character state. A multiple-rate model of evolution provided the best fit for mean distance between neuromasts, relative neuromast density and neuromast distribution area. However, a single-rate model of evolution provided the best fit for traits associated with neuromast numbers (table S6). Thus, the

444 evolutionary rate of cave-related neuromast patterns were highest in cave adapted
445 forms. Further, rates of evolution for surface area covered by SN neuromasts, and
446 right-sided neuromast numbers, are moderately increased in Blind and Micro-Eyed
447 species.

448 **Table 2.** Model-averaged rate parameters for the measured traits of neuromasts in
449 eyes-related morphs of *Sinocyclocheilus* species. **Bold font** = highest rate

450

Trait	Average rate		
	Blind	Micro-Eyed	Normal-Eyed
Number	155.1042	**179.4815**	150.6202
Left Number	**0.6395**	0.4106	0.4249
Right Number	**0.7095**	0.5056	0.5329
Area	102.8836	**106.2819**	101.9520
Mean distance	**34.4129**	11.7357	7.9001
Density	**362.2959**	64.3977	42.2944

451 **(g) Behavioural correlates of neuromasts**

452 We performed a series of behavioural assays, and found that Blind species
453 navigate markedly differently from eyed-species. Blind species have a well-
454 established wall-following behaviour, while sighted species utilize an entire arena
455 space (figure 5). We found that Blind species prefer to use the side with fewer
456 neuromasts for wall-following, but the side with more neuromasts for exploring (i.e.,
457 stimulation during VAB test). Micro-Eyed species having a left-bias in neuromast
458 distribution, and they preferred approaching the stimulation from the left-side (median
459 = 4) more frequently than right-side (median = 3; $W = 612$, $p > 0.05$). These species,
460 however, followed the wall on their right-side (median = 154) for a significantly
461 longer time compared to the left-side (median = 142; $W = 967$, $p < 0.001$; figure 5*c,g*;

table S5). Behavioural heatmaps depicting wall-following behaviour showed that Blind species prefer swimming in a fixed route, but eyed-species swam in irregular patterns (figure 5 *d-f'*). Wall following behaviour has also been characterized in *Astyanax mexicanus*. In this species, blind morphs similarly use the side with fewer neuromasts towards the wall, perhaps to use the contralateral side for detecting stimuli important for feeding, communication and spatial learning [17, 42].

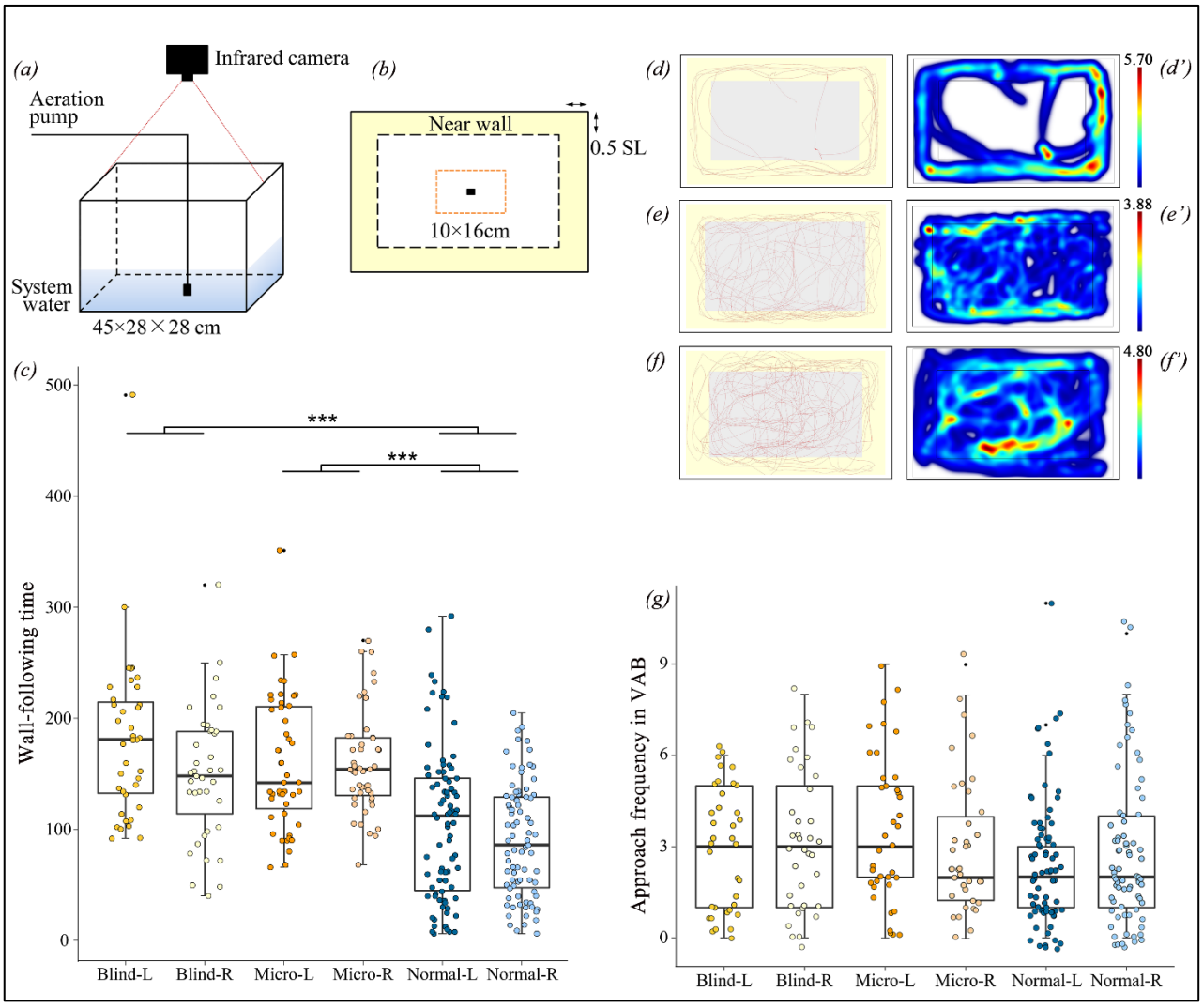

Figure 5. The experimental setup and results of the behavioural assays.

(a) Schematic diagram showing the assay system used to for the wall-following and vibration attraction behaviour (VAB).

(b) The vertical view of the arena's schematic diagram. The pale yellow area within the dotted line depict the near-wall belt ("Near wall"). The orange dotted line showed the stimulating area. The black rectangle in center shows the Aeration pump.

(c) The boxplot showing a comparison of the wall following time of Blind (3 species; n = 9), Micro-Eyed (4 species; n = 12) and Normal-Eyed (7 species; n = 21) morphs. Their handedness was also considered and the Kruskal-wallis Rank Sum Tests showed that the groups spent significantly different ($U = 79.49$, $p < 0.001$) times following the wall. Levels of significance indicated by ***.

(d-f'). Representative result of a 10-min wall-following behaviour assay for three species. Vertical view of the swimming path of Blind fish (d,d'; *S. tianeensis*, B-TB), Micro-Eyed fish (e,e'; *S. microphthalmus*, M-TB) and Normal-Eyed fish (f,f'; *S. macrophthalmus*, N-TB).

(d, e, f) Visualization of the traces of the fish swimming paths as depicted by EthoVision.

(d', e', f') Heatmaps generated from the trial results of the wall-following behaviour. The color bar represents the total time (min) the fish stayed in one place. Warmer colors denote areas with a longer time spent, whereas cooler colors denote areas of shorter time spent.

(g) The results of the frequency of approach in stimulation area of VAB test.

Sinocyclocheilus is an ancient species complex, with an estimated age for the clade of nearly 10-11 Mya [9, 62].They are distributed across an enormous karstic area spanning three provinces in China [21]. One of the main forms of speciation

494 seems to be isolation of populations over long periods, and therefore geographic
495 speciation appears to have dominated this diversification [61]. This divergence
496 occurred during the geological uplift of the Yunnan-Kweichow Plateau together with
497 the aridification of China, which occurred during the Pliocene and the Pleistocene
498 [61]. The neuromast variability seen in these fishes is most likely attributable to the
499 collective influences of both selection- and drift-related evolutionary mechanisms that
500 have played on these fishes over long periods. However, the exact dynamics of the
501 evolution of neuromasts is still an intriguing question to be explored.
502
503 **Conclusion**
504 In *Sinocyclocheilus,* alongside some basic patterns, there is widespread variation in
505 cephalic neuromast patterns between species and to some extent within species. We
506 showed neuromast asymmetry with right-side enhanced for most species. For almost
507 all species, the dorsal neuromast numbers were lesser than either of the sides.
508 Furthermore, Regressed-Eyed (Blind and Micro-Eyed) species are more asymmetric
509 than the Normal-Eyed forms. Interestingly, we found the greatest degree of neuromast
510 variation and rate of evolution in Micro-Eyed species (living outside and inside caves
511 - troglophilic), this is possibly an adaptation for life in two markedly different habitats
512 types. Assays of swimming behaviour suggest a functional role of neuromasts in
513 habitat exploration. These patterns of neuromast distribution and swimming
514 behaviours are convergent with other cavefish lineages. The diversity of patterns and

variation can be explained by the deep evolutionary history associated with the karstic region and the associated traits of this remarkable diversifications of fishes.

Abbreviations Section:

TB: Troglobitic; TP: Troglophilic; S: Surface; B: Blind; M: Micro-Eyed; N: Normal-Eyed; CN: Canal neuromast; SN: Superficial neuromast; GXU: Guangxi University; SL: Standard length; DEL: Delaunay Mean Distance (neuromast mean distance coefficient); L: Left-Side; R: Right-Side; D: Dorsal-Side; PCC: asymmetry coefficient 1 = Pearson's Correlation Coefficient; OC: asymmetry coefficient 2 = Overlap-Coefficient; PCA: Principal component analysis; AIC: Akaike information criterion; mtDNA: Mitochondrial DNA; ND4: NADH-ubiquinone oxidoreductase chain 4; Cyt b: cytochrome b gene.

Declarations

Acknowledgements: We thank the following individuals: members of EDD lab for their cooperation and support; Chenghai Fu for assistance in the field; Gajaba Ellepola for suggestions with the data analyses.

Funding

This work was supported by the (1) Startup funding for MM though Guangxi University for fieldwork, lab work and student support. (2) National Natural Science Foundation of China (#31860600) to JY for lab and fieldwork. (3) BC, TM and YL

were supported also by Innovation Project of Guangxi Graduate Education YCBZ2021008. These funding bodies played no role in the design of the study and collection, analysis, and interpretation of data or in the writing of the manuscript.

Conflicts of interest/Competing interests

We declare no conflicts of interest.

Ethics approval

The project was approved by Guangxi Autonomous Region Government and Guangxi University Ethical Clearance Committee (protocol number: GXU-2021-125).

Consent to participate

Not applicable.

Availability of data and material

All the data used in the study are provided in the electronic supplementary material.

Authors' contributions

Conceptualization – MM, BC, JBG; Fieldwork – YL, BC, TM, MM, JY; Experimentation and Lab Work – BC, XL, APR; Data Analyses – BC, TM, WD, XL; Interpretation – All; Figures – BC, WD, TM; Writing original draft – BC, MM, JBG, APR; Subsequent Drafts – All; Funding acquisition – MM, JY, BC, TM, YL;

559 Supervision – MM, JBG, JY.

560

561 ## References

562 1 Jeffery WR. 2001 Cavefish as a model system in evolutionary developmental biology. *Dev. Biol*. **231**,
563 1-12. (doi:10.1006/dbio.2000.0121)
564 2 Berti R, Durand JP, Becchi S, Brizzi R, Keller N, Ruffat G. 2001 Eye degeneration in the blind cave-
565 dwelling fish *Phreatichthys andruzzii*. *Can. J. Zool*. **79**, 1278-1285. (doi:10.1139/z01-084)
566 3 Jeffery WR. 2009 Regressive evolution in *Astyanax* cavefish. *Annu. Rev. Genet*. **43**, 25-47.
567 (doi:10.1146/annurev-genet-102108-134216)
568 4 Niemiller ML, Fitzpatrick BM, Miller BT. 2008 Recent divergence with gene flow in Tennessee cave
569 salamanders (Plethodontidae: *Gyrinophilus*) inferred from gene genealogies. *Mol. Ecol*. **17**, 2258-2275.
570 (doi:10.1111/j.1365-294X.2008.03750.x)
571 5 Jeffery WR, Strickler AG, Guiney S, Heyser DG, Tomarev SI. 2000 *Prox 1* in eye degeneration and
572 sensory organ compensation during development and evolution of the cavefish *Astyanax*. *Dev. Genes*
573 *Evol*. **210**, 223-230. (doi:10.1007/s004270050308)
574 6 Wilkens H, Strecker U. 2003 Convergent evolution of the cavefish *Astyanax* (Characidae, Teleostei):
575 genetic evidence from reduced eye-size and pigmentation. *Biol. J. Linn. Soc*. **80**, 545-554.
576 (doi:10.1111/j.1095-8312.2003.00230.x)
577 7 Yoshizawa M, Jeffery WR. 2011 Evolutionary tuning of an adaptive behavior requires enhancement
578 of the neuromast sensory system. *Commun. Integr. Biol*. **4**, 89-91. (doi:10.4161/cib.14118)
579 8 Yang JXet al.. 2016 The *Sinocyclocheilus* cavefish genome provides insights into cave adaptation.
580 *BMC Biol*. **14**, 1. (doi:10.1186/s12915-015-0223-4)
581 9 Mao TR, Liu YW, Meegaskumbura M, Yang J, Ellepola G, Senevirathne G, Fu C, Gross JB, Pie MR.
582 2021 Evolution in *Sinocyclocheilus* cavefish is marked by rate shifts, reversals, and origin of novel traits.
583 *BMC Ecol. Evol*. **21**, 45. (doi:10.1186/s12862-021-01776-y)
584 10 Cahn PH. 1989 The mechanosensory lateral line: neurobiology and evolution. *BioScience*. **40**, 215-
585 216. (doi:10.2307/1311373)
586 11 Webb JF, Shirey JE. 2003 Postembryonic development of the cranial lateral line canals and
587 neuromasts in zebrafish. *Dev. Dynam*. **228**, 370-385. (doi:10.1002/dvdy.10385)
588 12 Fritzsch B, Wahnschaffe U. 1983 The electroreceptive ampullary organs of urodeles. *Cell Tissue Res*.
589 **229**, 483-503. (doi:10.1007/BF00207693)
590 13 Smith S. 1996 Pattern formation in the urodele mechanoreceptive lateral line: What features can be
591 exploited for the study of development and evolution? *Int. J. Dev. Biol*. **40**, 727-733. (doi:10.1016/0141-
592 8130(96)01109-9)
593 14 Bird NC, Webb JF. 2014 Heterochrony, modularity, and the functional evolution of the
594 mechanosensory lateral line canal system of fishes. *EvoDevo*. **5**, 21. (doi:10.1186/2041-9139-5-21)
595 15 Gross JB, Gangidine A, Powers AK. 2016 Asymmetric facial bone fragmentation mirrors asymmetric
596 distribution of cranial neuromasts in blind Mexican cavefish. *Symmetry*. **8**, 118.
597 (doi:10.3390/sym8110118)
598 16 Elipot Y, Hinaux H, Callebert J, Rétaux S. 2013 Evolutionary shift from fighting to foraging in blind
599 cavefish through changes in the serotonin network. *Curr. Biol*. **23**, 1-10. (doi:10.1016/j.cub.2012.10.044)
600 17 Yoshizawa M. 2015 Behaviors of cavefish offer insight into developmental evolution. *Mol. Reprod.*

Dev. **82**, 268-280. (doi:10.1002/mrd.22471)

18 Jiang Y, Peichel CL, Torrance L, Rizvi Z, Thompson S, Palivela VV, Pham H, Ling F, Bolnick DI. 2017 Sensory trait variation contributes to biased dispersal of threespine stickleback in flowing water. *J. Evol. Biol*. **30**, 681-695. (doi:10.1111/jeb.13035)

19 Simon V, Hyacinthe C, Rétaux S. 2019 Breeding behavior in the blind Mexican cavefish and its river-dwelling conspecific. *PLoS ONE*. **14**, e0212591. (doi:10.1371/journal.pone.0212591)

20 Ma ZQ, Herzog H, Jiang YG, Zhao YH, Zhang DY. 2020 Exquisite structure of the lateral line system in eyeless cavefish *Sinocyclocheilus tianlinensis* contrast to eyed *Sinocyclocheilus macrophthalmus* (Cypriniformes: Cyprinidae). *Integr. Zool*. **15**, 314-328. (doi:10.1111/1749-4877.12430)

21 Romero A, Zhao YH, Chen XY. 2009 The hypogean fishes of China. *Environ. Biol. Fishes*. **86**, 211-278. (doi:10.1007/s10641-009-9441-3)

22 Zhao YH, Zhang CG. 2009 *Endemic fishes of Sinocyclocheilus (Cypriniformes: Cyprinidae) in China -- Species diversity, cave adaptation, systematics and zoogeography*. Beijing: Science Press.

23 Webb JF, Northcutt RG. 1997 Morphology and distribution of pit organs and canal neuromasts in non-teleost bony fishes. *Brain Behav. Evol*. **50**, 139-151. (doi:10.1159/000113328)

24 Powers AK, Berning DJ, Gross JB. 2020 Parallel evolution of regressive and constructive craniofacial traits across distinct populations of *Astyanax mexicanus* cavefish. *J. Exp. Zool. B Mol. Dev. Evol*. **334**, 450-462. (doi:10.1002/jez.b.22932)

25 George PL, Borouchaki H. 1998 *Delaunay triangulation and meshing: application to finite elements*. Paris: Hermès.

26 Aurenhammer F, Klein R, Lee D-T. 2012 *Voronoi diagrams and delaunay triangulations*. World Scientific.

27 Lee DT, Schachter BJ. 1980 Two algorithms for constructing a delaunay triangulation. *Int. J. Parallel Program*. **9**, 219-242. (doi:10.1007/BF00977785)

28 Palmer AR, Strobeck C, Chippindale AK. 1993 Bilateral variation and the evolutionary origin of macroscopic asymmetries. *Genetica*. **89**, 201-218. (doi:10.1007/BF02424514)

29 Gorlewicz A, Krawczyk K, Szczepankiewicz AA, Trzaskoma P, Mulle C, Wilczynski GM. 2020 Colocalization colormap – an ImageJ Plugin for the quantification and visualization of colocalized signals. *Neuroinformatics*. **18**, 661-664. (doi:10.1007/s12021-020-09465-9)

30 Zeitvogel F, Schmid G, Hao L, Ingino P, Obst M. 2016 ScatterJ: An ImageJ plugin for the evaluation of analytical microscopy datasets. *J. Microsc*. **261**, 148-156. (doi:10.1111/jmi.12187)

31 Cordelières F, Bolte S. 2008 JACoP v2.0: improving the user experience with co-localization studies. *ImageJ User & Developer Conference*. 174-181.

32 Wang YS, Wu QH, Hu MQ, Liu B, Chai ZY, Huang R, Wang Y, Xu HD, Zhou L, Zheng LH*, et al.* 2017 Ligand- and voltage-gated Ca2+ channels differentially regulate the mode of vesicular neuropeptide release in mammalian sensory neurons. *Sci. Signal*. **10**, eaal1683. (doi:10.1126/scisignal.aal1683)

33 Bolte S, Cordelières FP. 2007 A guided tour into subcellular colocalization in light microscopy. *J. Microsc*. **224**, 213-232. (doi:10.1111/j.1365-2818.2006.01706.x)

34 Dunn KW, Kamocka MM, McDonald JH. 2011 A practical guide to evaluating colocalization in biological microscopy. *Am. J. Physiol. Cell Physiol*. **300**, C723-C742. (doi:10.1152/ajpcell.00462.2010)

35 Manders EM, Stap J, Brakenhoff GJ, van Driel R, Aten JA. 1992 Dynamics of three-dimensional replication patterns during the S-phase, analysed by double labelling of DNA and confocal microscopy. *J. Cell Sci*. **103**, 857-862. (doi:10.1242/jcs.103.3.857)

36 Zinchuk V, Grossenbacher Zinchuk O. 2009 Recent advances in quantitative colocalization analysis:

focus on neuroscience. *Prog. Histochem. Cytochem*. **44**, 125-172. (doi:10.1016/j.proghi.2009.03.001)

37 Huelsenbeck JP, Ronquist F, Nielsen R, Bollback JP. 2001 Bayesian inference of phylogeny and its impact on evolutionary biology. *Science*. **294**, 2310-2314. (doi:10.1126/science.1065889)

38 Revell LJ. 2012 Phytools: an R package for phylogenetic comparative biology (and other things). *Methods Ecol. Evol*. **3**, 217-223. (doi:10.1111/j.2041-210X.2011.00169.x)

39 Planidin NP, Reimchen TE. 2021 Ecological predictors of lateral line asymmetry in stickleback (*Gasterosteus aculeatus*). *Evol. Ecol*. **35**, 609-629. (doi:10.1007/s10682-021-10117-w)

40 Sharma S, Coombs S, Patton P, de Perera TB. 2009 The function of wall-following behaviors in the Mexican blind cavefish and a sighted relative, the Mexican tetra (*Astyanax*). *J. Comp. Physiol. A*. **195**, 225-240. (doi:10.1007/s00359-008-0400-9)

41 Patton P, Windsor S, Coombs S. 2010 Active wall following by Mexican blind cavefish (*Astyanax mexicanus*). *J. Comp. Physiol. A*. **196**, 853-867. (doi:10.1007/s00359-010-0567-8)

42 Burt de Perera T, Braithwaite VA. 2005 Laterality in a non-visual sensory modality — the lateral line of fish. *Curr. Biol*. **15**, 241-242. (doi:10.1016/j.cub.2005.03.035)

43 Jiang YG, Fu JC, Zhang DY, Zhao YH. 2016 Investigation on the lateral line systems of two cavefish: *Sinocyclocheilus Macrophthalmus* and *S. Microphthalmus* (Cypriniformes: Cyprinidae). *J. Bionic Eng*. **13**, 108-114. (doi:10.1016/S1672-6529(14)60164-5)

44 McGaugh SE, Weaver S, Gilbertson EN, Garrett B, Rudeen ML, Grieb S, Roberts J, Donny A, Marchetto P, Gluesenkamp AG. 2020 Evidence for rapid phenotypic and behavioural shifts in a recently established cavefish population. *Biol. J. Linn. Soc*. **129**, 143-161. (doi:10.1093/biolinnean/blz162)

45 Dezfuli BS, Magosso S, Simoni E, Hills K, Berti R. 2009 Ultrastructure and distribution of superficial neuromasts of blind cavefish, *Phreatichthys andruzzii*, juveniles. *Microsc. Res. Tech*. **72**, 665-671. (doi:10.1002/jemt.20714)

46 Powers AK, Kaplan SA, Boggs TE, Gross JB. 2018 Facial bone fragmentation in blind cavefish arises through two unusual ossification processes. *Sci. Rep*. **8**, 7015. (doi:10.1038/s41598-018-25107-2)

47 Soares D, Niemiller ML. 2020 Variation in cephalic neuromasts surface and cave-dwelling fishes of the family amblyopsidae (teleostei: percopsiformes). *J. Cave Karst Stud*. **82**, 198-209. (doi:10.4311/2019LSC0115)

48 Trokovic N, Herczeg G, Ghani NIA, Shikano T, Merilä J. 2012 High levels of fluctuating asymmetry in isolated stickleback populations. *BMC Evol. Biol*. **12**, 115. (doi:10.1186/1471-2148-12-115)

49 Soares D, Niemiller ML. 2020 Extreme Adaptation in Caves. *Anat. Rec*. **303**, 15-23. (doi:10.1002/ar.24044)

50 Krishnan J, Rohner N. 2017 Cavefish and the basis for eye loss. *Philos. Trans. R. Soc. Lond., B. Biol. Sci*. **372**, 20150487. (doi:10.1098/rstb.2015.0487)

51 Fernandes VFL, Macaspac C, Lu L, Yoshizawa M. 2018 Evolution of the developmental plasticity and a coupling between left mechanosensory neuromasts and an adaptive foraging behavior. *Dev. Biol*. **441**, 262-271. (doi:10.1016/j.ydbio.2018.05.012)

52 Coombs S, Janssen J, Webb JF. Year Diversity of lateral line systems: evolutionary and functional considerations. In: J. Atema, R. R. Fay, A. N. Popper, W. N. Tavolga, editors. Sensory Biology of Aquatic Animals; 1988; New York, NY: Springer New York; 1988. 553-593.

53 Montgomery JC, Coombs S, Baker CF. 2001 The mechanosensory lateral line system of the hypogean form of *Astyanax Fasciatus*. *Environ. Biol. Fishes*. **62**, 87-96. (doi:10.1023/A:1011873111454)

54 Yamamoto Y, Byerly MS, Jackman WR, Jeffery WR. 2009 Pleiotropic functions of embryonic *sonic hedgehog* expression link jaw and taste bud amplification with eye loss during cavefish evolution. *Dev.*

Biol. **330**, 200-211. (doi:10.1016/j.ydbio.2009.03.003)

55 Zhao YH, Zhang CG. 2006 Past research and future development on endemic Chinese cavefish of the genus *Sinocyclocheilus* (Cypriniformes, Cyprinidae). *Acta Zootaxonomica Sinica*. **31**, 769-777.

56 He Y, Chen XY, Xiao TQ, Yang JX. 2013 Three-dimensional morphology of the *Sinocyclocheilus hyalinus* (Cypriniformes : Cyprinidae) horn based on synchrotron X-ray microtomography. *Zool. Res*. **34**, 128-134. (doi:10.11813/j.issn.0254-5853.2013.E4-5.E128)

57 Teyke T. 1990 Morphological differences in neuromasts of the blind cave fish *Astyanax hubbsi* and the sighted river fish *Astyanax mexicanus*. *Brain Behav. Evol*. **35**, 23-30. (doi:10.1159/000115853)

58 Wark AR, Peichel CL. 2010 Lateral line diversity among ecologically divergent threespine stickleback populations. *J. Exp. Biol*. **213**, 108-117. (doi:10.1242/jeb.031625)

59 Zhao YH, Watanabe K, Zhang CG. 2006 *Sinocyclocheilus donglanensis*, a new cavefish (Teleostei: Cypriniformes) from Guangxi, China. *Ichthyol. Res*. **53**, 121-128. (doi:10.1007/s10228-005-0317-z)

60 Culver D, Pipan T. 2019 *The biology of caves and other subterranean habitats*.

61 Xiao H, Chen SY, Liu ZM, Zhang RD, Li WX, Zan RG, Zhang YP. 2005 Molecular phylogeny of *Sinocyclocheilus* (Cypriniformes: Cyprinidae) inferred from mitochondrial DNA sequences. *Mol. Phylogenet. Evol*. **36**, 67-77. (doi:10.1016/j.ympev.2004.12.007)

62 Li ZQ, Guo BC, Li JB, He SP, Chen YY. 2008 Bayesian mixed models and divergence time estimation of Chinese cavefishes (Cyprinidae: *Sinocyclocheilus*). *Chinese Science Bulletin*. **53**, 2342-2352. (doi:10.1007/s11434-008-0297-2)